High methane emissions from a eutrophic marine coastal basin driven by bubble release from the sediment

Olga M. Żygadłowska[1], Jessica Venetz[2], Wytze K. Lenstra[1,2], Niels A.G.M. van Helmond[1,2], Robin Klomp[1,2], Thomas Röckmann[3], Annelies J. Veraart[4], Mike S.M. Jetten[2], Caroline P. Slomp[1,2]

[1] Department of Earth Sciences - Geochemistry, Utrecht University, The Netherlands

[2] Department of Microbiology, Radboud Institute for Biological and Environmental Sciences, Radboud University, Nijmegen, The Netherlands

[3] Institute for Marine and Atmospheric Research Utrecht, Utrecht University, Utrecht, The Netherlands

[4] Department of Aquatic Ecology and Environmental Biology, Radboud Institute for Biological and Environmental Sciences, Radboud University, Nijmegen, The Netherlands

Correspondence:

Olga M. Żygadłowska

o.m.zygadlowska@uu.nl

Keywords: methane oxidation, coastal ecosystem, iron, oxygen, deoxygenation

Running head: High methane emissions from a coastal basin

Author Contribution Statement:

Olga M. Zygadlowska: Data curation (equal); formal analysis (lead); investigation (equal); methodology (equal); visualization (lead); writing – original draft (lead); writing – review and editing (lead). **Jessica Venetz:** Data curation (equal); formal analysis (equal); investigation (equal); methodology (equal); writing – review and editing (equal); **Wytze K. Lenstra:** Data curation (supporting); formal analysis (supporting); investigation (equal); methodology (equal); writing – review and editing (equal); **Niels A.G.M. van Helmond:** Data curation (supporting); investigation (equal); methodology (equal); writing – review and editing (equal); **Robin Klomp:** data curation (supporting); investigation (equal); methodology (equal); writing – review and editing (equal); **Thomas Röckmann:** investigation (supporting); methodology (equal); writing – review and editing (equal); **Annelies Veraart:** conceptualization (equal); investigation (equal); methodology (supporting); writing – review and editing (equal); **Mike S.M. Jetten:** conceptualization (equal); data curation (equal); funding acquisition (equal); investigation (equal); project administration (equal); supervision (supporting); writing – review and editing (equal); **Caroline P. Slomp:** conceptualization (equal); data curation (equal); formal analysis (supporting); funding acquisition (equal); investigation (equal); methodology (equal); project administration (equal); supervision (lead); writing - original draft (supporting); writing – review and editing (equal).

Abstract

The production of methane in coastal sediments and its release to the water column is intensified by anthropogenic eutrophication and bottom water hypoxia, and it is yet uncertain whether methane emissions to the atmosphere will be enhanced. Here, we assess seasonal variations in methane dynamics in a eutrophic, seasonally euxinic coastal marine basin (Scharendijke, Lake Grevelingen). In-situ benthic chamber incubations reveal high rates of methane release to the water column (74 – 163 mmol m^{-2} d^{-1}) between March and October 2021. Comparison of in-situ benthic and calculated diffusive fluxes indicates that methane was primarily released in the form of bubbles. In spring and fall, when the water column was oxic, most of the dissolved methane was removed aerobically in the bottom water. In early summer, in contrast, methane accumulated below the oxycline. Enrichments in $\delta^{13}C–CH_4$ and δD-CH_4 and the abundant presence of methane oxidizing bacteria point towards removal of methane around the oxycline, possibly linked to iron oxide reduction. Methane emissions to the atmosphere were substantial in all seasons with the highest, in-situ measured diffusive chamber fluxes (1.2 mmol m^{-2} d^{-1}) observed upon the onset of temperature-induced mixing at the end of summer. Methane release events in the floating chamber and model calculations point towards a high year-round flux of methane to the atmosphere in the form of bubbles (55 - 120 mmol m^{-2} d^{-1}), which bypass the microbial methane filter. Because of bubble formation methane emissions from eutrophic coastal systems are likely higher than previously thought.

Introduction

Methane is a potent greenhouse gas with a global warming potential 28 times higher than that of carbon dioxide on a time scale of 100 years (IPCC 2007). In the past century, the atmospheric concentration of methane has been increasing, reaching a new record of 1921 ppb in 2023 (Lan et al. 2023). In addition to anthropogenic sources, the global methane budget is also greatly impacted by natural sources of methane, including marine environments. Coastal systems are of particular interest since they contribute up to 75 % of the total marine methane flux to the atmosphere (Rosentreter et al. 2021) despite accounting for only 15 % of the marine surface area (Weber et al. 2019). Coastal environments worldwide are increasingly affected by eutrophication and deoxygenation (Breitburg et al. 2018). While such environments are frequently characterized by high methane concentrations in the water column (e.g. Reeburgh et al. 1991; Gelesh et al. 2016), it remains unclear what fraction of the methane ultimately escapes to the atmosphere (Naqvi et al. 2010; Weber et al. 2019; Saunois et al. 2020).

Methane is produced in anoxic sediments during organic matter degradation (Froelich et al. 1979) and can be removed through both aerobic and anaerobic pathways (Reeburgh 2007; Wallenius et al. 2021). Anaerobic pathways in sediments include methane oxidation coupled to the reduction of sulfate (Knittel and Boetius 2009), iron and manganese oxides (Beal et al. 2009; Sivan et al. 2011; Ettwig et al. 2016) and nitrate (Ettwig et al. 2009; Haroon et al. 2013). The efficiency of methane removal in sediments is especially sensitive to the environmental setting. High rates of sediment accumulation and input of organic matter in particular can lead to such high rates of methane production that the slow-growing anaerobic methanotrophs cannot keep up (Dale et al. 2008; Egger et al. 2016; Lenstra et al. 2023). This may lead to a shoaling of the zone of methane production and enhanced release of methane to the water column (Egger et al. 2016; Lenstra et al. 2023). When the production of methane exceeds the

rate of its diffusive transport, this results in oversaturation of dissolved methane in porewaters and the formation of methane bubbles (Boudreau et al. 2005; Schmid et al. 2017). Methane in the form of bubbles can bypass the sedimentary microbial filter and directly escape into the water column (Judd et al. 1997; Leifer and Patro 2002; Joye et al. 2004).

Dissolved methane and methane bubbles differ in their dominant pathway of vertical transport in the water column. Transport of dissolved methane is controlled by turbulent diffusion as a result of density-driven (temperature and salinity dependent) convection or wind-induced mixing (Imboden and Wüest 1995; Read et al. 2012). When rates of turbulent diffusion are high and the water column is fully mixed, methane can be mixed upward rapidly. Such well-mixed water columns are typically also oxygenated. In stratified water columns, however, rates of turbulent diffusion will be low around the pycnocline, promoting the development of an oxycline, i.e. a transition from oxic to anoxic waters with water depth, frequently allowing accumulation of methane below the oxycline (Gelesh et al. 2016; Steinsdóttir et al. 2022). Vertical transport of methane in bubbles primarily depends on the bubble diameter and the water depth of bubble release, with smaller bubbles and deeper waters promoting dissolution of methane in the water column (McGinnis et al. 2006). From the viewpoint of methane removal, such dissolution is critical since methane bubbles are not subject to microbial oxidation.

Removal of dissolved methane primarily involves aerobic methane-oxidizing bacteria, and anaerobic methane-oxidizing bacteria and archaea. In a water column where an oxycline is present, most methane is expected to be removed by methane oxidizing bacteria in the zone where methane directly meets oxygen (Schmale et al. 2010; Steinle et al. 2017; Venetz et al. 2023a). Recent work has shown that methane oxidizing bacteria can also be active in anoxic

waters and utilize electron acceptors other than oxygen. Such removal of methane below the oxycline has been linked to aerobic methanotrophic bacteria of the *Methylococcales* family, with the methane oxidation being coupled to partial denitrification (Padilla et al. 2017; Steinsdóttir et al. 2022). In a recent study for freshwater sediments, these aerobic methanotrophs were also found to couple methane oxidation to iron(III) reduction (Li et al. 2023), but whether this holds for coastal marine waters is not known. Potential anaerobic methanotrophs include "Candidatus *Methanoperedens*" of the archaeal ANME-2d cluster, which are known to link methane oxidation to nitrate, iron(III) and manganese(IV) reduction (Ettwig et al. 2010, 2016; Leu et al. 2020) and Ca. *Methylomirabilis*, which produces the oxygen needed for methane oxidation through dismutation of nitric oxide from nitrite reduction (Ettwig et al. 2010; Padilla et al. 2016; Thamdrup et al. 2019). While Ca. *Methylomirabilis* were found to be actively oxidizing methane in the waters of oxygen minimum zones (Padilla et al. 2016), this does not hold for Ca. *Methanoperedens*, although the latter have been reported to be present in low abundance in at least two coastal systems (Thamdrup et al. 2019; Venetz et al. 2023a; Żygadłowska et al. 2023).

Progressive eutrophication of coastal systems is expected to enhance the methane flux from sediments (Crill and Martens 1987; Gelesh et al. 2016; Lenstra et al. 2023). Eutrophication not only enhances the rate of methane production in the sediment, it also reduces the rate of bubble dissolution in the water column because larger bubbles are formed (McGinnis et al. 2006) which are more resistant to dissolution (Delwiche and Hemond 2017). Hence, the chance of methane bubbles reaching the atmosphere is particularly high in eutrophic systems (Boudreau et al. 2005) with shallow waters (< 100 m; McGinnis et al. 2006; Ostrovsky et al. 2008). Despite the large potential for bubble-associated methane release in coastal areas, we know very little about the contribution of bubbles to methane emissions in these regions.

In this study, we quantify benthic release of methane and assess the seasonal changes in methane concentrations and microbial removal in the water column in a eutrophic, seasonally stratified and euxinic marine basin (Lake Grevelingen, Netherlands) between March and October 2021. We pay specific attention to the microbial removal of methane near the oxycline. Using floating chamber incubations at the water-air interface and diffusive flux calculations, we assess the seasonality in methane emissions. We find that methane release from the sediment is high throughout the year, and mostly occurs in the form of bubbles. While methane that is dissolved is efficiently removed by aerobic methanotrophs, a large proportion of the methane bypasses the microbial methane filter in the water column in the form of bubbles and escapes to the atmosphere.

Materials and methods

Study area

Marine Lake Grevelingen is a former estuary of the river Rhine that was dammed at the landward side in 1964 and at the North Sea side in 1971. While the average depth of the lake is 5.1 m, it is intersected by much deeper former tidal channels. Sluices in the dam at the seaward side are opened regularly since 1978, setting the lake salinity to relatively constant values of 29 to 33. The lake is highly eutrophic and the water column in the main channel is subject to temperature-induced stratification and bottom water hypoxia or anoxia every summer since at least 1978 (Hagens et al. 2015). In this study, we focus on the deepest basin of the lake (Scharendijke basin; 45 m water depth; 51.742°N, 3.849°E) located close to the seaward dam (Egger et al. 2016). The Scharendijke basin is seasonally euxinic with strong water column stratification between May and September and high release of methane from the sediment to the water column (Egger et al. 2016; Żygadłowska et al. 2023). High

concentrations of methane in the bottom waters (74 μmol L^{-1}) were previously observed at the end of the stratification period in September 2020, with most of the methane oxidation occurring near the oxycline primarily attributed to microbes of the *Methylomonadaceae* family (Venetz et al. 2023a). Maximum diffusive methane fluxes to the atmosphere were estimated to be 0.37 mmol m^{-2} d^{-1} (Żygadłowska et al. 2023).

Sampling of the water column and sediment as well as in-situ benthic and floating chamber deployments were performed during 9 sampling campaigns on board RV Navicula between March and October 2021. Depth profiles of dissolved oxygen, temperature and salinity were obtained using a CTD (Seabird SBE 911 plus) equipped with an oxygen sensor (Seabird SBE43). Common methods used to determine oxygen concentrations in seawater (sensors, Winkler titrations) suffer from a background signal and artefacts in oxygen-depleted waters (Grégoire et al. 2021). Here, we consider oxygen to be absent when concentrations are close to zero and the profile becomes a vertical line.

Porewater methane sampling

During each sampling campaign, two sediment cores were collected using a UWITEC gravity corer and transparent PVC core liners (120 cm length, 6 cm inner diameter). Methane samples were collected from the first core immediately after retrieval using a liner with two lines of holes drilled at 5 cm intervals on opposite sides of the liner offset by 2.5 cm and covered with tape. From each hole, 10 mL of sediment was taken with a cut-off plastic syringe and transferred into a 65 mL glass bottle filled with saturated NaCl solution. The bottles were topped up with NaCl, closed with rubber stoppers and aluminum screw caps and stored upside down until analysis. Note that methane degassing may occur during sample collection, leading to an underestimation of methane concentrations (Egger et al. 2017; Jørgensen et al. 2019). This effect intensifies with higher concentrations of methane, but does not significantly impact

its isotopic composition (Wallace et al. 2000; Egger et al. 2017). A second sediment core was sliced to determine porosity based on the weight loss upon oven-drying, assuming a sediment density of 2.65 g cm^{-3}.

Water column sampling

Water samples were collected using a 10 L Niskin bottle at a depth resolution of 1-2 m during each sampling campaign on board RV Navicula. Samples were collected for the analysis of methane and its isotopic composition ($\delta^{13}C$-CH_4 and δD-CH_4), sulfide, ammonium, nitrate, nitrite and total and dissolved metals. Serum bottles of 120 mL were used to collect methane samples. The bottles were filled from the bottom up with water directly taken from the Niskin bottle and were allowed to overflow. The bottles were closed with butyl rubber stoppers and crimped with aluminum caps ensuring that no air bubbles remained inside. All samples were poisoned with a 0.25 mL saturated mercury chloride solution directly after collection, and stored upside down in the dark.

Water column samples for sulfide, ammonium, nitrite and nitrate were filtered through 0.2 μm nylon syringe filters. The sulfide samples were taken by adding 0.5 mL sample to glass vials pre-filled with 2 mL 2% zinc acetate solution and afterwards stored at 4 °C. The samples for ammonium, nitrate and nitrite were directly stored at -20 °C. Total dissolvable (henceforth termed “total”) and dissolved iron and manganese samples were collected directly from the Niskin bottle into 250 mL LDPE Nalgene bottles using Tygon 5000 tubing. The Nalgene bottles and tubing were acid washed prior to sampling to avoid trace metal contamination (Cutter et al. 2017). The acid washing procedure consisted of two overnight baths at 60 ºC in 5 % decon and 10 % HCl, respectively. After each bath the bottles and tubing were rinsed 5 times with MilliQ. In the last step the Nalgene bottles were filled up with 0.1 % HCl and kept in an oven at 60 ºC overnight. After complete cooling the bottles were emptied and packed for

further use. The samples used to determine the dissolved fractions of iron and manganese were filtered directly from the Niskin bottle using a 0.2 μm Sartobran 300 cartridge filter. Both unfiltered and filtered samples were then acidified with concentrated ultrapure HCl (200 μL of acid per 100 mL of sample). The samples for total iron and manganese were filtered with a 0.45 μm nylon filter exactly 6 months after collection, to ensure that the exposure time of the particles to acid was identical for each set of the unfiltered samples.

In-situ benthic and sea-air methane flux measurements

In-situ benthic fluxes of methane were measured using a MiniChamber Lander System (Unisense) equipped with a metal-free polycarbonate incubation chamber (30 x 30 x 35 cm) and a set of twelve 50 mL plastic syringes controlled by an autosampler and connected to the chamber with plastic tubing. The adjustable feet of the lander enabled the incubation chamber to sink 7 cm into the sediment, leaving a water volume in the chamber of 25.2 L, which, together with its surface area of 0.09 m^2, was used to calculate the in-situ benthic fluxes of methane. The lid of the incubation chamber was open for 10 minutes after the lander was placed at the sea floor allowing any resuspended sediment to settle before sampling started. A stirrer attached to the lid constantly mixed the water in the chamber to keep the incubated water homogeneous. The stirring is also expected to dissolve methane bubbles that are released from the sediments and enter the chamber. Each deployment consisted of 5 timepoints (25 to 30 minutes apart from each other). For each timepoint two syringes were filled to ensure enough water was collected to allow the sample vials for methane to overflow. A small septum in the lid of the chamber ensured replacement of the water that was withdrawn. Upon retrieval the samples were transferred to 65 mL serum bottles, closed with rubber stopper and an aluminum screw cap, poisoned with 0.1 mL of saturated mercury chloride solution and stored upside down in the dark until analysis.

In-situ sea-air methane fluxes were measured with a floating chamber (Venetz et al. in prep). The transparent acrylic cylindric floating chamber (390 mm diameter), was connected to a LICOR trace gas analyzer (LI-7810) forming a closed loop. Fluxes were measured in triplicate, with each measurement lasting 3 to 10 minutes, until a linear change was observed. The chamber was ventilated after each measurement until atmospheric methane concentrations were reached. The wind speed and temperature were determined during each measurement and were used to calculate methane fluxes. Instances of sudden increases in methane concentrations due to bubbles entering the chamber occurred during 5 sampling cruises. Those data were removed from the diffusive flux calculations and, instead, were used to estimate the order of magnitude of the bubble flux. The bubble flux was estimated based on the change of methane concentrations in the chamber and the number of bubble events per sampling campaign. Due to high winds, deployments of the benthic and floating chambers were not possible in May.

Chemical analysis

To determine methane concentrations in the pore water, water column and lander samples, 10 mL of nitrogen gas was added to each sample while simultaneously removing the same volume of liquid. Methane concentrations were measured with a Thermo Finnigan Trace™ gas chromatograph (Flame Ionization Detector; limit of detection 0.02 μmol L^{-1}) following gas and water phase equilibration (>2h for water column samples and 7 days for sediment samples). The analysis of stable methane isotopes (δ^{13}C-CH_4 and δD-CH_4) was conducted using Continuous Flow Isotope Ratio Mass Spectrometry (CF-IRMS) as described by Brass and Röckmann (2010) and Sapart et al. (2011).

Sulfide concentrations were determined using the phenylenediamine and ferric chloride method (Cline 1969). The indophenol blue method (Solorzano 1969) was used to measure ammonium. Nitrite and nitrate concentrations were determined with a Gallery™ Automated

Chemistry Analyzer type 861 (Thermo Fisher Scientific). The total and dissolved concentrations of iron and manganese were determined by inductively coupled plasma mass spectrometry (ICP-MS, Perkin Elmer NexION 2000). The samples were concentrated in order to remove the seawater matrix using a SC-DX SeaFAST S2 (Elemental Scientific) prior to analysis (Lenstra et al. 2022). The samples, previously acidified to pH 2, were loaded onto a pre-concentration column (20 s) after being buffered with glacial acetic acid (4.8 M, 99.7 %, Baseline, Seastar) and ammonium hydroxide (4.1 M, 29 %, Baseline, Seastar). The analyte was measured online upon direct injection into the device. The recovery for iron and manganese was 96 % and 93 %, respectively, and the average limit of detection, determined as three times the standard deviation of the analysis of oligotrophic seawater with known trace metal concentrations, was 0.1 and 0.3 nmol L^{-1}, respectively. For both iron and manganese, the dissolved fraction was slightly higher than the total fraction in the sulfidic waters below 35 m. This is likely an analytical artifact due to high sulfide concentrations as observed previously (Lenstra et al. 2021).

Methanotrophs

To obtain insight in the vertical distribution of methanotrophs in the water column, samples for DNA analysis were collected in March, July, August, end of August and October and filtered through 0.22 μm PES Supor filters using a vacuum pump. The filters were stored at -80 ºC directly after collection. The DNA collected on the filters was extracted using a FastDNA™ SPIN Kit for Soil DNA isolation kit (MP Biomedicals). Microbial community composition at each depth was analyzed by sequencing the V3-V4 region of the 16S rRNA gene (Ilumina MiSeq platform, Macrogen) as described in Venetz et al. (2023a).

Calculations

The total amount of oxygen, sulfide, ammonium and methane in the water column per m^2 during each sampling campaign was calculated by integrating the concentrations of each compound with water depth. We distinguish three sections of the water column, namely the top 0-15 m, middle 15-35 m and bottom 35-45 m. In-situ benthic fluxes of methane were calculated from the change in concentration of methane in the chamber, using linear regression and accounting for the volume of the chamber and its area (Supporting information, Figure S1). Diffusive fluxes of methane across the sediment-water interface were calculated according to Fick's first law:

$$J = -\phi D_s \frac{dC}{dz} \qquad \text{(Equation 1)}$$

where J is the diffusive flux in mmol m^{-2} d^{-1}, ϕ is the porosity of the sediment, D_s is the diffusion coefficient for methane in the sediment in m^{-2} d^{-1}, C is the concentration of methane in the porewaters in mmol L^{-1} and z is the sediment depth in m. Ds is calculated from the diffusion coefficient for methane in seawater, corrected for salinity and temperature using the R package CRAN: *marelac* (Soetaert et al. 2010), accounting for the tortuosity of the sediment (Boudreau 1996).

The in-situ fluxes of methane at the water-atmosphere interface were calculated using the following equation:

$$CH_4\ atmospheric\ flux_{in-situ} = \frac{\Delta CH_4}{\Delta t} \times \frac{V}{A} \qquad \text{(Equation 2)}$$

where ΔCH_4 is the change of the amount of methane in the chamber (mmol) over given time interval Δt (d), V is the volume of the chamber (m^3) and A is the area of the chamber (m^2). A more detailed description of the procedure can be found in Venetz et al. (in prep).

The diffusive fluxes of methane across the water-atmosphere interface were determined based on the following equation:

$$F_{atm} = k(C_W - C_O) \quad \text{(Equation 3)}$$

where F_{atm} represents the diffusive flux from the water column to the atmosphere in mmol m^{-2} d^{-1}, k is the gas exchange coefficient in m d^{-1}, C_W is the dissolved methane concentration at 1 m depth in μmol L^{-1}, and C_O is the calculated methane concentration in equilibrium with the atmosphere in μmol L^{-1}. The dissolved concentrations of methane in seawater (C_W) and air (C_O) were calculated as:

$$C_W = xCH_{4sw}\, \beta\, \rho \quad \text{(Equation 4)}$$

$$C_O = xCH_{4atm}\, \beta\, \rho \quad \text{(Equation 5)}$$

where xCH_{4sw} and xCH_{4atm} are the measured molar fractions of methane in sea water and atmosphere in nmol mol^{-1}, β represents the Bunsen solubility coefficient (dimensionless) and ρ is the atmospheric pressure in bars. The Bunsen solubility coefficient is calculated from Wiesenburg and Guinasso (1979) as:

$$ln\beta = A1 + A2\left(\frac{100}{T}\right) + A3\ln\left(\frac{T}{100}\right) + S[(B1 + B2\left(\frac{T}{100}\right) + B3\left(\frac{T}{100}\right)^2] \quad \text{(Equation 6)}$$

where A1, A2, A3, B1, B2 and B3 are constants, T is the temperature in K and S is salinity. The gas exchange coefficient (k) is determined according to Wanninkhof (2014):

$$k = 0.251\, U^2 \left(\frac{Sc}{600}\right)^{-0.5} \quad \text{(Equation 7)}$$

where U is the wind speed in m s^{-1}, Sc is the Schmidt number (dimensionless), the quotient of kinematic viscosity of seawater in m^2 s^{-1} which is dependent on temperature and salinity (Pilson 2013) and the diffusion coefficient of methane in seawater in m^2 s^{-1}, dependent on temperature (Jähne et al. 1987). The minimum and maximum wind speed data for each sampling day were obtained from the Royal Netherlands Meteorological Institute database for a nearby coastal meteorological station (station Hoek van Holland; https://www.knmi.nl/nederland-nu/klimatologie/daggegevens).

The range of the ebullitive methane flux to the atmosphere was estimated from the benthic bubble flux of methane, the water depth of the basin and an assumed diameter of the methane bubbles, based on model results described by McGinnis et al. (2006). The model provides an estimate of the percentage of the methane that dissolves in the water column (with the remainder then being emitted to the atmosphere) based on the water depth and bubble size at a given site. The bubble flux of methane from the sediment in Scharendijke basin was calculated as the difference between the in-situ lander flux and the calculated diffusive flux. The basin has a water depth of 45 m. The diameter of the bubbles was assumed to be 20 mm. This implies that the bubble emission to the atmosphere at our site ranges from 0 to 75 % of the initial bubble flux at the sediment-water interface meaning that 25 to 100 % of the bubbles dissolve in the water column before they can reach the atmosphere. Therefore the maximum flux of methane bubbles to the atmosphere can be estimated as 75 % of the flux of methane bubbles at the sediment-water interface.

Results

Water column salinity, temperature and oxygen

The salinity in Scharendijke basin increased slightly with water depth from values around 29 in the surface waters to ca. 31 at depth and showed little change throughout the year (Figure 1). This contrasted strongly with the large seasonal changes in temperature and oxygen. While in March and April, the water column still had a constant temperature of around 8 ºC and was oxygenated, temperature-induced density stratification led to the formation of three distinct layers in the water column from May onwards, with a warm, oxic surface layer (0 to 15 m) overlying a colder, a middle layer with variable oxygen content (15 to 35 m) and an even colder, anoxic bottom layer (35 to 45 m). In August and September, the temperature throughout the water column gradually increased, indicating the beginning of mixing. In October, the water column was fully mixed again as evident from the uniform temperatures of around 15 ºC and the abundant presence of oxygen at all water depths.

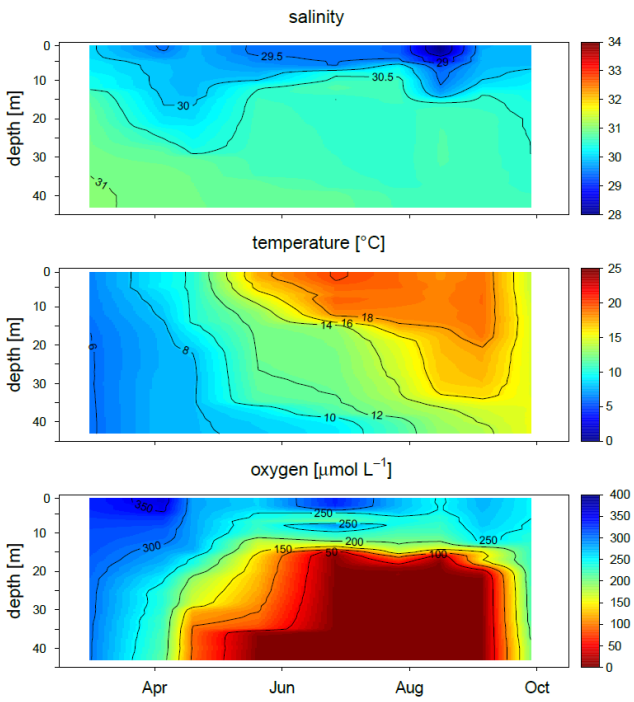

Figure 1. Seasonal dynamics of salinity, temperature and oxygen in the water column between March and October 2021 in the Scharendijke basin (Lake Grevelingen).

Benthic release of methane

The in-situ benthic fluxes of methane measured with the lander were high during all sampling campaigns, with the highest flux from the sediment into the water column observed in March (163 mmol m^{-2} d^{-1}; Table 1; Supporting information, Figure S2). Porewater concentrations of methane were high throughout the year (Supporting information, Figure S1). Calculated diffusive fluxes of methane from the sediment to the bottom water ranged from 0.7 to 3.8 mmol m^{-2} d^{-1} (Table 1) and hence can account for only a minor fraction of the in-situ measured benthic fluxes. Although there was quite some variability in the calculated diffusive flux, there was no distinct trend with time.

Table 1. Diffusive and total in-situ fluxes of methane at the sediment-water interface, diffusive and in-situ fluxes of methane to the atmosphere and estimated flux of methane bubbles to the atmosphere. All fluxes are given in mmol m^{-2} d^{-1}. N.a.: not available.

Sampling date	In-situ benthic flux of methane	Diffusive flux of methane at the sediment-water interface	In-situ flux of methane to the atmosphere	Calculated diffusive methane flux to the atmosphere (min. and max.)	Maximum flux of methane bubbles to the atmosphere based on McGinnis et al. (2006) model
March	162.9	2.9	0.01	0.02 – 0.10	120
April	73.9	1.1	0.66	0.08 – 1.46	55
May	n.a.	3.8	n.a.	0.02 – 0.14	n.a.
June	109.4	1.8	0.12	0.03 – 0.54	81
July	123.4	2.1	0.22	0.02 – 0.35	91
August	93.5	2.0	0.17	0.00 – 0.12	69
Aug/Sept	126.4	0.7	0.96	0.65 – 1.33	94
September	99.7	1.1	1.15	0.20 – 1.10	74
October	104.0	3.7	0.38	0.12 – 0.31	75

Water column depth profiles

The stratification of the water column not only contributed to the development of anoxia but also allowed for the accumulation of hydrogen sulfide in the bottom layer, i.e. below 35 m

(Figure 2). While in June the oxycline was present at a depth of 35 m, the anoxia expanded upwards to a depth of around 15-20 m in summer, leading to the development of a suboxic, i.e. anoxic and non-sulfidic, zone. Hydrogen sulfide was continuously present in the bottom water layer of the water column throughout the summer, at variable concentrations, ranging from 54 to 141 μmol L^{-1}, until full mixing of the water column in October.

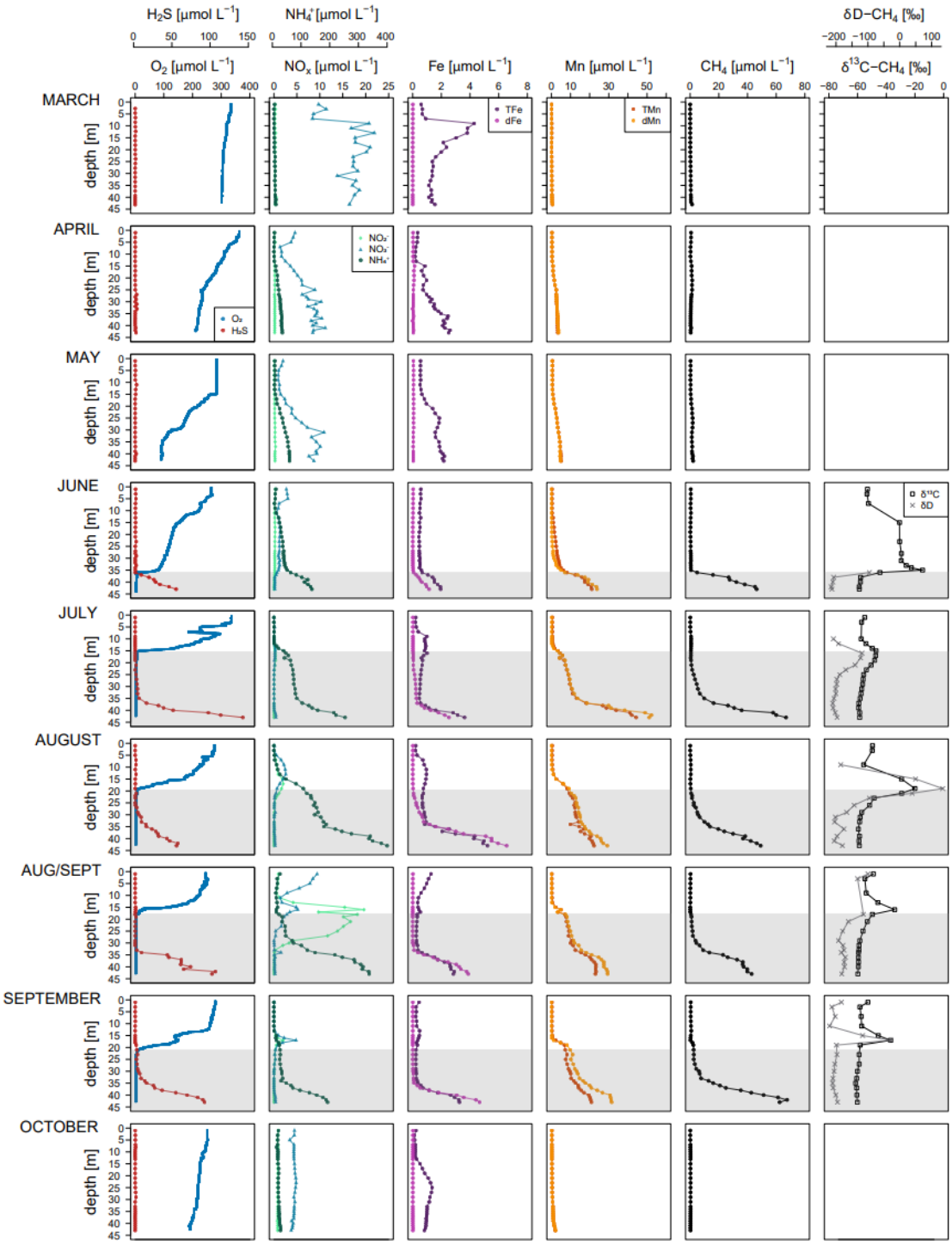

Figure 2. Water column depth profiles of oxygen, sulfide, nitrate, nitrite, ammonium, total dissolvable (Td) and dissolved (d) iron and manganese, methane and methane isotopes (δ^{13}C given in ‰ vs. VPDB (Vienna Pee Dee Belemnite); δD given in ‰ vs. V-SMOW (Vienna Standard Mean Ocean Water) of each sampling between March and October 2021.

Concentrations of ammonium, nitrate and nitrite in the water column showed a distinct seasonality. While ammonium was near zero in March, it accumulated in the lower and middle part of the water column from April to August, when a maximum concentration of 400 μmol L^{-1} was reached (Figure 2). From the end of August onwards, ammonium concentrations gradually decreased again, especially in the middle part of the water column. Mixing of the water column in October led to a return to ammonium concentrations close to zero at all water depths. Nitrate concentrations, in contrast, were highest from March to May and in October, and, with the exception of the waters near the oxycline in August and September when a maximum was observed near the oxycline, were mostly low in summer. Nitrite also showed a pronounced maximum near the oxycline in August and September, with concentrations up to 20 μmol L^{-1}. At other times of the year, nitrite was largely absent.

Dissolved iron concentrations were low from March to May and in October. From June onwards, however, substantial dissolved iron was present in the waters below the oxycline, especially in the bottom layer below 35 m depth. Total iron, which is a measure of both dissolved and particulate iron, showed an even more distinct seasonality, with elevated concentrations in the oxic water column between March and May and in October, indicating a relatively high abundance of particulate iron in the water column at this time. In July and August, particulate iron was also present above and/or below the oxycline.

Depth profiles of total and dissolved manganese were very similar, indicating that most manganese was present in dissolved form. With the exception of March, dissolved manganese concentrations increased with depth in the water column with the highest concentrations occurring from June to September, i.e. in the months in which an oxycline was present.

Table 2. Date of sample collection, water depth at which oxygen was depleted (oxycline depth) and surface and bottom water concentrations of methane for water samples collected with the Niskin bottle. N.a.: not applicable.

	Oxycline depth [m]	**CH_4 [µmol L^{-1}]**	
Sampling date		**Surface waters**	**Bottom waters**
March	n.a.	0.04	1.37
April	n.a.	0.24	0.15
May	n.a.	0.11	0.80
June	36	0.16	17.38
July	15	0.10	66.87
August	20	0.06	49.17
Aug/Sept	18	0.25	42.90
September	22	0.40	62.41
October	n.a.	0.10	0.24

Water column methane concentrations were low between March and May but methane strongly accumulated below the oxycline from June to September, with a maximum bottom water value of 68 μmol L^{-1}. Methane concentrations in the surface water varied considerably throughout the year, with the highest values observed in September, at the end of August and in April (0.4, 0.3 and 0.2 μmol L^{-1}, respectively; Table 2). A strong increase in $\delta^{13}C - CH_4$ and in $\delta D - CH_4$ was seen near the oxycline from June to September, with the highest values observed in June ($\delta^{13}C - CH_4$: -15 ‰) and in August ($\delta D - CH_4$: 127 ‰) (Figure 2). While the isotopic enrichment for methane was restricted to waters above the oxycline in June and September, this did not hold for July and August; in the profiles for these months, most of the increase was

observed below the oxycline. The methane isotopic signatures of the surface water differed from those around the oxycline and were largely similar to those in the bottom water.

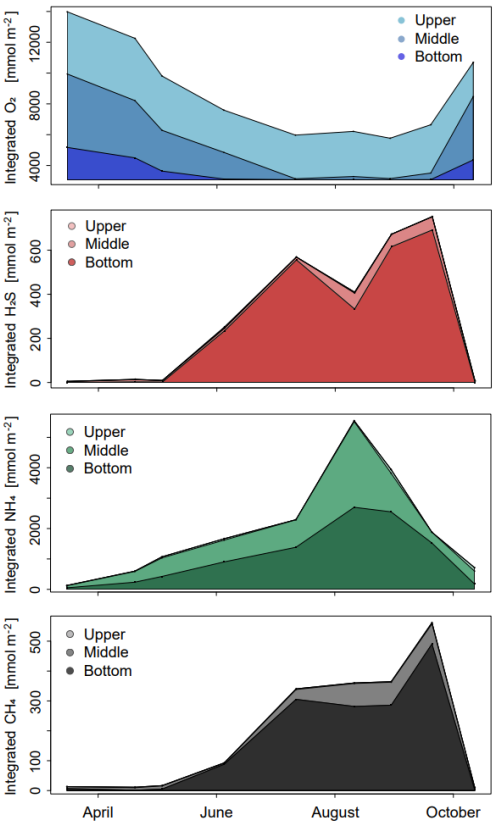

Figure 3. Integrated water column concentrations of oxygen, sulfide, ammonium and methane in the upper, middle and bottom parts of the water column between March and October 2021. The upper layer refers to depths between 0 to 15 m, the middle layer to depths between 15 and 35 m and the lower layer to depths between 35 and 45 m.

The integrated concentrations of oxygen, hydrogen sulfide, ammonium and methane in the water column for March to October (Figure 3) highlight the strong seasonal changes in water column chemistry. While oxygen was nearly completely lost from the middle and bottom layers of the water column from July to September, sulfide primarily accumulated in the bottom layer, in line with the development of a suboxic zone at this time. After an initial rise in sulfide, ammonium and methane upon the onset of anoxia in June, the accumulation of the solutes

became more variable from July onwards. Most of the solutes were lost from the water column again upon full water column mixing in October.

Relative abundance of methane oxidizing bacteria

The methanotrophic community in the water column was dominated by methane oxidizing bacteria within the family of the *Methylomonadaceae*. In March, only a small number of 16S rRNA gene reads affiliated to methane oxidizing bacteria was observed in the water column. The abundance of the methane oxidizing bacteria increased upon stratification and the development of anoxia in the middle and lower part of the water column (Figure 4). The methane oxidizing bacteria were mostly found near and below the oxycline. In October, the abundance of methane oxidizing bacteria increased with depth, with the highest relative abundance observed near the sediment-water interface. The relative abundance of methane oxidizing bacteria in the upper 10 m of the water column was low in all of the five months that were used for 16S rRNA analysis.

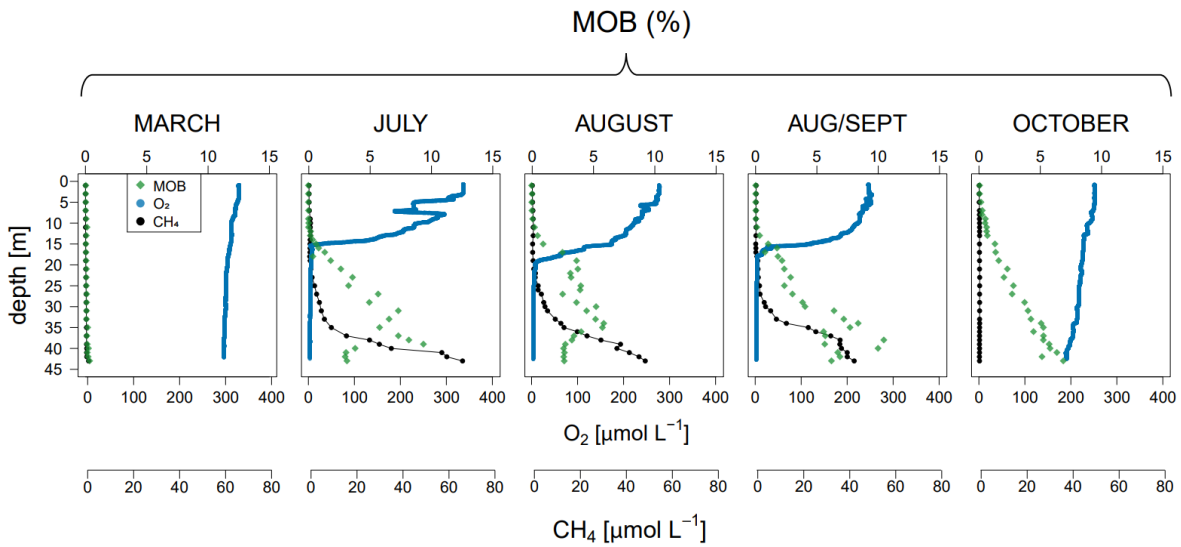

Figure 4. The abundance of methane oxidizing bacteria (MOB) relative to the total abundance of all bacteria in the water column determined in the 16S sequencing procedure in March, July, August, end of August and September 2021, and the oxygen and methane profiles in the water column from Fig. 2 for reference.

In-situ and calculated fluxes of methane to the atmosphere

The in-situ diffusive flux of methane from the water column to the atmosphere measured with the floating chamber ranged from 0.01 to 1.15 mmol m^{-2} d^{-1} and was highly variable throughout the year (Table 1, Figure 5). The highest flux was observed in April and at the end of August and in September, while the lowest fluxes were measured in March and June. The calculated diffusive flux of methane to the atmosphere was of the same order of magnitude as the in-situ measured flux and showed a similar trend with time. The estimated maximum bubble flux to the atmosphere ranged from 55 to 120 mmol m^{-2} d^{-1} (Table 1). The events of bubbles entering the floating chamber during measurements were highly variable and irregular throughout the year. The average bubble flux based on these events amounted to 67 mmol m^{-2} d^{-1} (Supporting information, Table S2).

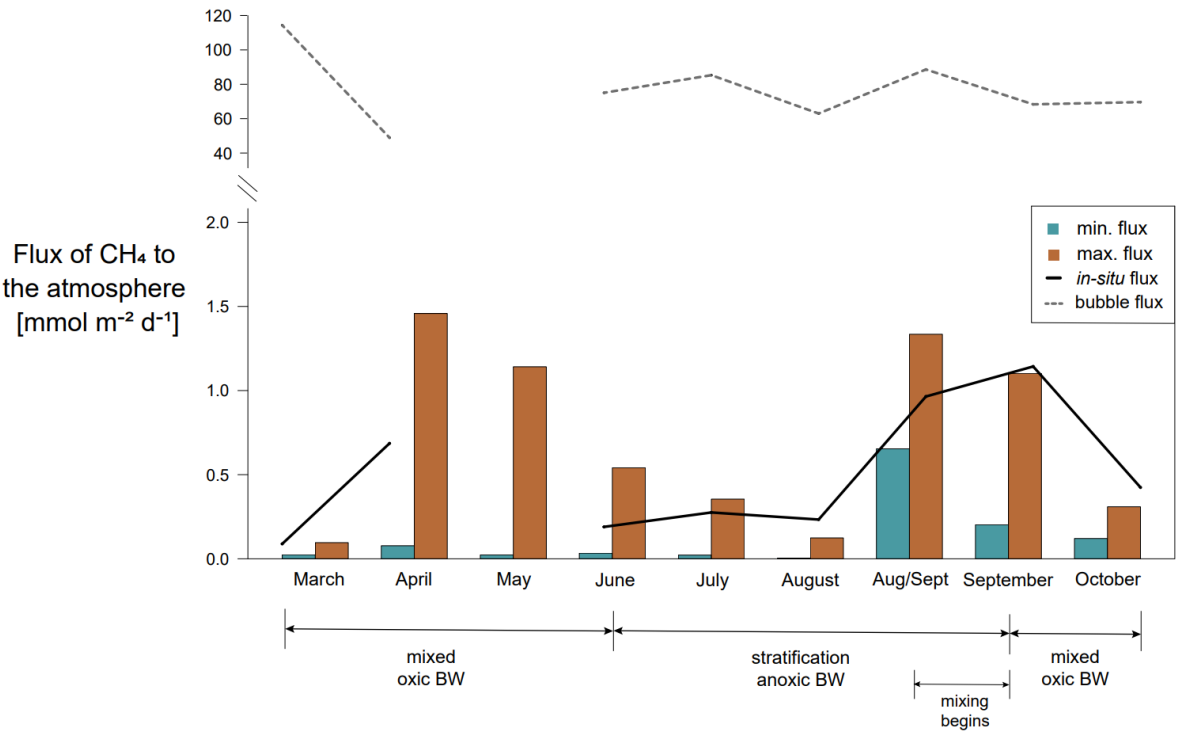

Figure 5. Minimum and maximum diffusive fluxes of methane to the atmosphere calculated according to equation 1. In-situ sea-air fluxes of methane were measured with floating chambers. The bubble fluxes to the atmosphere were estimated based on the bubble release from the sediment, assuming a large bubble size (20 mm).

Discussion

High benthic release of methane in the form of bubbles

Lake Grevelingen receives large amounts of algal material from the adjacent North Sea in summer. This contributes to its highly eutrophic state (Hagens et al. 2015) and supports high rates of methane production in the sediments in the deeper areas of the lake (Egger et al. 2016). We find that rates of in-situ benthic methane release in Scharendijke basin are high throughout the year and, on average, are equal to ca. ~110 mmol m^{-2} d^{-1}. Importantly, the average diffusive flux of methane across the sediment-water interface, which is calculated from the concentration change in dissolved methane in the porewater of the surface sediment and the bottom water, was only 2 mmol m^{-2} d^{-1}. Hence, diffusion was responsible for only a minor fraction of the total methane release from the sediments which implies that a large proportion of the methane must be escaping into the water in the form of bubbles.

The methane fluxes observed here are, although high, not unreasonable as the input of organic matter to the sediments at this site is known to be at least a factor two higher: reactive transport modeling of porewater ammonium profiles points towards an organic matter input of ~250 mmol C m^{-2} d^{-1} (Egger et al. 2016). Nonetheless, to our knowledge, these in-situ benthic fluxes (74 – 163 mmol m^{-2} d^{-1}) are higher than those observed so far in other eutrophic coastal systems. For example, benthic methane fluxes of up to 9 mmol m^{-2} d^{-1} and up to 35 mmol m^{-2} d^{-1} were observed for the eutrophic coastal systems of Cape Lookout Bight (Klump and Martens 1980) and Puck Bay (Reindl and Bolałek 2014), respectively. Our observed methane fluxes are closer to rates seen in freshwater lakes, such as, for example, the shallow eutrophic Lake Wohlen, for which a total benthic ebullition flux of 51 mmol m^{-2} d^{-1} was observed (DelSontro et al. 2015). This illustrates that eutrophication may allow for much higher benthic fluxes of methane from coastal sediments, than commonly considered. Importantly, Scharendijke basin has a marine

salinity of ~30, implying that the abundant presence of sulfate as an electron acceptor does not safeguard coastal systems against high rates of benthic methane release.

Organic matter input into Scharendijke basin differs seasonally, with higher inputs in summer. Bottom water redox conditions also vary seasonally, with bottom water euxinia establishing in summer (Figure 2; Egger et al. 2016; Zygadlowska et al. 2023). The in-situ benthic flux of methane (Table 1) does not follow such a seasonal pattern, however. Hence, the fluctuations in the benthic flux throughout the year are unlikely the result of temporal changes in rates of methanogenesis and methane removal linked to variations in bottom water redox conditions or organic matter input but are rather the result of spatial variations within the basin. We note that the benthic flux driven by bubbles may be especially variable due to the stochastic nature of bubble release (Bastviken et al. 2004; Wik et al. 2013). Notably, our results contrast with those of a recent study of fjord sediments in which reoxygenation of surface sediments led to a lower benthic methane fluxes (Bonaglia et al. 2022). This may be due to a lower contribution of ebullition in the fjord sediments. At Scharendijke, most methane escapes in the form of bubbles and therefore can bypass the benthic microbial filter, regardless of the bottom water redox state. To allow for such a high bubble flux persistently throughout the year, methane must be oversaturated in the pore waters and methane production must always exceed methane oxidation. This highlights the role of eutrophication as a key driver of methane release to the water column: above a certain site-dependent threshold, all additional methane produced may bypass the zone of methanotrophic oxidation and will be released to the water column in the form of bubbles.

Seasonality in methane removal pathways

The dynamics of dissolved methane in the water column of the Scharendijke basin were strongly affected by temperature-driven stratification during the summer months. The

stratification of the water column not only limited the downward supply of oxygen but also allowed hydrogen sulfide, ammonium and methane to accumulate in the middle and deeper water (Figure 3). Even though stratification persisted throughout the summer, the trends in hydrogen sulfide and methane in the bottom layer between July and August (Figure 2 and 3) suggest removal of these reduced compounds. We hypothesize that part of this removal was linked to a lateral inflow event of oxygenated water from the North Sea (Hagens et al. 2015), starting in July. We also see a weakening of water column stratification because of warming of the water column, allowing for an enhanced downward supply of oxygen and upward transport of reduced substances in the summer months, prior to the full mixing that occurred in October.

The depth profiles of methane isotopes (Figure 2) and methane oxidizing bacteria (Figure 4), reveal seasonal variations in the depths where methane was microbially removed. In March and October, the relative abundance of the methane oxidizing bacteria was highest in the bottom water and in the lower part of the water column, respectively, This points towards aerobic removal of methane. Nevertheless, relatively high methane concentrations (0.04 to 0.24 μmol L^{-1}), were still found in the surface waters in spring (Table 2). This is likely the result of upward mixing of methane in the well-mixed water column.

In June, the distinct counter gradients in oxygen and methane and strong enrichment in $\delta^{13}C$ – CH_4 and δD–CH_4 at the oxycline (Figure 2) point towards aerobic removal. Aerobic methanotrophy is common in many stratified systems (Mau et al. 2013; Reis et al. 2020) and was observed at the oxycline in the water column of Scharendijke basin previously (Zygadlowska et al. 2023; Venetz et al. 2023a). In July and August, however, the oxycline was located at a shallower depth, and enrichments in $\delta^{13}C$ – CH_4 and δD – CH_4 were observed in

the suboxic zone below the oxycline, suggesting methane removal in the absence of oxygen. However, as noted above, it is likely that there still was oxygen supply to this zone through both vertical and lateral transport, implying that some of the methane removal could still be aerobic. Notably, the enrichment of particulate iron near the oxycline and increase of dissolved iron below the oxycline (Figure 2) point towards active iron cycling, as is common in anoxic, sulfide-free zones in anoxic basins (Millero 1991). While no methanotrophic archaea were present, high numbers of methane oxidizing bacteria of the *Methylomonadaceae* were observed below the oxycline (Figure 4). These seemingly aerobic microbes have also been found to be capable of methane oxidation coupled to iron oxide reduction in oxygen-deprived conditions (Li et al. 2023). Hence, we conclude that in July and August, the *Methylomonadaceae* may have been involved in both aerobic and anaerobic removal of methane, with the latter process possibly linked to iron reduction. Again, some methane was present in the surface waters (0.06 - 0.25 μmol L^{-1}), indicating incomplete removal of methane.

At the end of August and in September, the stratification weakened further and the water column slowly began to mix (Figure 6). The physical mixing of the water column enhanced upward transport of methane resulting in high surface water methane concentrations (0.25 and 0.4 μmol L^{-1}). *Methylomonadaceae* were still abundant below the oxycline, indicating there could have been methane removal below the oxycline as well. This was likely aerobic, since there is no evidence for iron cycling at this time (Figure 2). High concentrations of nitrate and nitrite were observed in the suboxic zone at the end of August, which likely resulted from a sudden nitrification event. Notably, there was no sign of *Methanomirabilis oxyfera* – the methanotrophs that can couple methane oxidation to nitrite reduction (Ettwig et al. 2010).

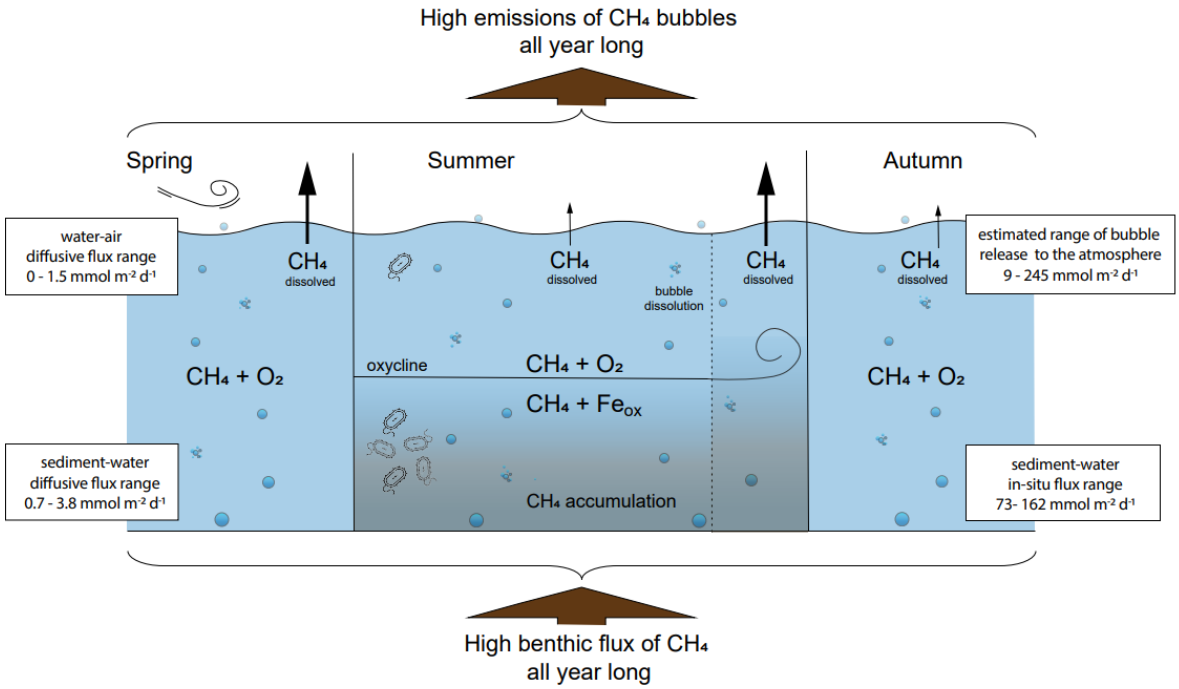

Figure 6. Schematic of methane dynamics at the Scharendijke basin. In spring the release of dissolved methane to the atmosphere is enhanced by wind-mixing. Summer stratification acts as a barrier and traps methane in the bottom waters, decreasing its diffusive release to the atmosphere. The breaking of stratification at the end of summer leads to release of the accumulated methane and results in high diffusive fluxes of methane to the atmosphere. Methane bubble emissions are high all year round regardless of the water column dynamics.

The isotopic fractionation factors calculated for the zone where enrichments in $\delta^{13}C - CH_4$ were observed in the summer ranged from 1.006 to 1.014 (Supporting information, Table S1). These values are within the lower range of fractionation factors reported for aerobic and anaerobic methane oxidation (1.002 – 1.035; Grant and Whiticar 2002). The fractionation factors are likely strongly affected by bubble dissolution since dissolving bubbles are expected to shift the isotopic signature towards more depleted values (Leonte et al. 2018). While concurrent changes in $\delta^{13}C$ and δD of methane point towards methane oxidation, a shift in $\delta^{13}C$ of methane is only observed at low methane concentrations in the water column (Figure 2;

Supporting information, Figure S3), in line with a control of methane transport in the water column by physical processes.

Table 3. Estimation of the contribution of bubble dissolution to methane concentrations at 5 m depth based on the methane isotope data and mass balance (Supporting information, Equation S1).

Date	**Methane concentration at 5m (μmol L^{-1})**	**Contribution from diffusion (μmol L^{-1})**	**Contribution from bubble dissolution**	
			(μmol L^{-1})	**(%)**
June	0.11	0.07	0.04	37
July	0.74	0.07	0.67	91
August	0.44	0.03	0.41	94
Aug/Sept	0.13	0.03	0.10	78
September	0.58	0.07	0.51	87

Bubble dissolution may have contributed to the relatively high methane concentrations found in the surface waters. In summer, we observe $\delta^{13}C$ – CH_4 and δD-CH_4 values above the oxycline similar to those in the bottom water. Using a mass balance (Supporting information, equation S1) we estimate that bubble dissolution accounts for up to 90% of the methane at a water depth of 5 m (Table 3). Although the concentrations found in the surface waters are generally low, when compared to the rest of the water column, this suggests that bubble dissolution plays a critical role in methane supply to the surface waters and, subsequently, the release of methane to the atmosphere. Apparently, methane oxidizing bacteria were unable to establish in the surface waters between March and October and hence were not able to efficiently remove the methane despite unlimited oxygen availability.

High methane fluxes to the atmosphere

The measured in-situ diffusive fluxes of methane to the atmosphere and the calculated diffusive fluxes of methane to the atmosphere were not only of the same order of magnitude, but also showed the same seasonal trend (Figure 5). All the fluxes were relatively high (on average 0.08 – 1 mmol m^{-2} d^{-1}) when compared to the average flux of methane to the atmosphere for continental shelves (0.03 mmol m^{-2} d^{-1}; Bange et al. 1994), which is in line with the highly eutrophic nature of our system. We find the highest fluxes in spring, when the water column was still well-mixed, and upon the onset of mixing of the stratified water column from end of August onwards. The high release in spring is in line with previous work showing that upward transport of dissolved methane can be very efficient in well-mixed water columns and can support high fluxes of methane to the atmosphere (Borges et al. 2016). Enhanced release of methane to the atmosphere after a period of stratification was previously observed in Chesapeake Bay (Gelesh et al. 2016) where very similar surface water concentrations (0.4 μmol L^{-1}) and diffusive fluxes (1.8 mmol m^{-2} d^{-1}) were observed.

At our site, the vast majority of methane is released from the sediments in the form of bubbles, however, and, of the total benthic flux of methane, only 0.5 % is emitted to the atmosphere via diffusion (Table 1). The efficiency of the microbial filter in the water column is therefore highly dependent on the extent of dissolution of the methane bubbles. If all the methane bubbles would dissolve in the water column, the efficiency of the microbial filter would on average amount to 99.5 %. Based on the benthic release of methane we estimated that the maximum flux of methane bubbles to the atmosphere (assuming that all the bubbles are large and have a diameter of 20 mm) ranges from 55 to 120 mmol m^{-2} d^{-1}. This rate of methane emission is approximately 100 times higher than methane emission via diffusion only (Table 1). The flux would be smaller if we assume smaller bubbles. However, high bubble fluxes and a large bubble diameter are known to correlate (Delwiche and Hemond 2017), indicating that with such high bubble fluxes

as found at Scharendijke, the formation of large bubbles is likely. Bubbles with a diameter larger than 10 mm not only carry more methane within their volume but are also much more resistant to dissolution and rise faster through the water column than smaller bubbles. This increases their chances of reaching the atmosphere without losing much methane on the way (DelSontro et al. 2015).

To further assess the role of bubble dissolution below the oxycline, we also applied a 1-dimensional model to the methane profiles for 5 key months assuming upward transport of methane by turbulent diffusion only (Crank 1975). We find that the measured depth profiles of methane in the water column do not differ to a great extent from the modelled profiles, especially in the bottom layer (Supporting information, Figure S4). This suggests that bubble dissolution indeed plays a relatively minor role in the stagnant layer below 35 m. While the rate of bubble dissolution may be similar throughout the water column, its role as a source of methane is more important in the surface waters where methane concentrations are generally much lower.

The average bubble flux throughout the year, estimated based on the bubbles caught in the floating chamber during the measurements was 67 mmol m^{-2} d^{-1} (Supporting information, Table S2) which is of the same order of magnitude as the maximum bubble fluxes estimated based on the benthic bubble release (Table 1). The estimated bubble flux is also comparable to bubble fluxes reported for the highly eutrophic Dalian Bay (74 mmol m^{-2} d^{-1}, Kunpeng et al. 2019), and slightly higher than that found in eutrophic Lake Wohlen (45 mmol m^{-2} d^{-1}; DelSontro et al. 2015).

We conclude that in the Scharendijke basin a large proportion of the methane released from the sediment is bypassing the microbial filter in the water column in the form of bubbles and is released directly to the atmosphere at high rates throughout the year. As deoxygenation and eutrophication advance, a growing number of coastal environments may witness a shift towards conditions in which methane bubbles account for the major proportion of the benthic methane flux and methane emissions to the atmosphere. As a consequence, the role of coastal systems as a source of methane to the atmosphere will increase in future.

Acknowledgements

We thank the captain and crew of the R/V Navicula, Y. Witte and other staff of the Royal Netherlands Institute for Sea Research (NIOZ) for their support during the sampling campaigns. We are also grateful to J. Visser, H. de Waard, T. Claessen, C. van der Veen, E. Heiskanen, R. Puyk and Y. Chung for analytical assistance in Utrecht. This research was financially supported by ERC Synergy grant MARIX (8540088). This work was carried out under the program of the Netherlands Earth System Science Center (NESSC 024002001) and SIAM 024002002, financially supported by the Ministry of Education, Culture and Science (OCW). The authors declare that the research was conducted in the absence of any commercial or financial relationships that could be construed as a potential conflict of interest.

References

Bange, H. W., U. H. Bartell, S. Rapsomanikis, and M. O. Andreae. 1994. Methane in the Baltic and North Seas and a reassessment of the marine emissions of methane. North **8**: 465–480. doi:10.1029/94GB02181

Bastviken, D., J. Cole, M. Pace, and L. Tranvik. 2004. Methane emissions from lakes: Dependence of lake characteristics, two regional assessments, and a global estimate. Global Biogeochem. Cycles **18**: 1–12. doi:10.1029/2004GB002238

Beal, E. J., C. H. House, and V. J. Orphan. 2009. Manganese-and iron-dependent marine methane oxidation. Science (80-.). **325**: 184–187. doi:10.1126/science.1169984

Bonaglia, S., T. Rütting, M. Kononets, A. Stigebrandt, I. R. Santos, and P. O. J. Hall. 2022. High methane emissions from an anoxic fjord driven by mixing and oxygenation. Limnol. Oceanogr. Lett. **7**: 392–400. doi:10.1002/lol2.10259

Borges, A. V., W. Champenois, N. Gypens, B. Delille, and J. Harlay. 2016. Massive marine methane emissions from near-shore shallow coastal areas. Sci. Rep. **6**: 2–9. doi:10.1038/srep27908

Boudreau, B. P. 1996. The diffusive tortuosity of fine-grained unlithified sediments. Geochim. Cosmochim. Acta **60**: 3139–3142. doi:10.1016/0016-7037(96)00158-5

Boudreau, B. P., C. Algar, B. D. Johnson, and others. 2005. Bubble growth and rise in soft sediments. Geology **33**: 517–520. doi:10.1130/G21259.1

Brass, M., and T. Röckmann. 2010. Continuous-flow isotope ratio mass spectrometry method for carbon and hydrogen isotope measurements on atmospheric methane. Atmos. Meas. Tech. **3**: 1707–1721. doi:10.5194/amt-3-1707-2010, 2010

Breitburg, D., L. A. Levin, A. Oschlies, and others. 2018. Declining oxygen in the global ocean and coastal waters. Science (80-.). **359**. doi:10.1126/science.aam7240

Cline, J. D. 1969. Spectrophotometric determination of hydrogen sulfide in natural waters 1. Limnol. Oceanogr. **14**: 454–458. doi:10.4319/lo.1969.14.3.0454

Crank, J. 1975. The mathematics of diffusion, 2nd Edn. Oxford University Press.

Crill, P. M., and C. S. Martens. 1987. Biogeochemical cycling in an organic-rich coastal marine basin. 6. Temporal and spatial variations in sulfate reduction rates. Geochim. Cosmochim. Acta **51**: 1175–1186. doi:10.1016/0016-7037(87)90210-9

Cutter, G. A., K. Casciotti, P. Croot, W. Geibert, L.-E. Heimbürger, M. C. Lohan, H. Planquette, and T. van de Flierdt. 2017. Sampling and sample-handling protocols for GEOTRACES Cruises, Version 3.0.

Dale, A. W., P. Van Cappellen, D. R. Aguilera, and P. Regnier. 2008. Methane efflux from marine sediments in passive and active margins : Estimations from bioenergetic reaction – transport simulations. Earth Planet. Sci. Lett. **265**: 329–344. doi:10.1016/j.epsl.2007.09.026

Delsontro, T., D. F. McGinnis, B. Wehrli, and I. Ostrovsky. 2015. Size does matter: Importance of large bubbles and small-scale hot spots for methane transport. Environ. Sci. Technol. **49**: 1268–1276. doi:10.1021/es5054286

Delwiche, K. B., and H. F. Hemond. 2017. Methane Bubble Size Distributions, Flux, and Dissolution in a Freshwater Lake. Environ. Sci. Technol. **51**: 13733–13739. doi:10.1021/acs.est.7b04243

Egger, M., W. Lenstra, D. Jong, and others. 2016. Rapid sediment accumulation results in high methane effluxes from coastal sediments. PLoS One **11**: 1–22. doi:10.1371/journal.pone.0161609

Egger, M., M. Hagens, C. J. Sapart, and others. 2017. Iron oxide reduction in methane-rich deep Baltic Sea sediments. Geochim. Cosmochim. Acta **207**: 256–276. doi:10.1016/j.gca.2017.03.019

Ettwig, K. F., T. Van Alen, K. T. van de Pas-Schoonen, M. S. M. Jetten, and M. Strous. 2009. Enrichment and molecular detection of denitrifying methanotrophic bacteria of the NC10 phylum. Appl. Environ. Microbiol. **75**: 3656–3662. doi:10.1128/AEM.00067-09

Ettwig, K. F., M. K. Butler, D. Le Paslier, and others. 2010. Nitrite-driven anaerobic methane oxidation by oxygenic bacteria. Nature **464**: 543–548. doi:10.1038/nature08883

Ettwig, K. F., B. Zhu, D. Speth, J. T. Keltjens, M. S. M. Jetten, and B. Kartal. 2016. Archaea catalyze iron-dependent anaerobic oxidation of methane. Proc. Natl. Acad. Sci. U. S. A. **113**: 12792–12796. doi:10.1073/pnas.1609534113

Froelich, P. N., G. P. Klinkhammer, M. L. Bender, and others. 1979. Early oxidation of organic matter in pelagic sediments of the eastern equatorial Atlantic: suboxic diagenesis. Geochim. Cosmochim. Acta **43**: 1075–1090. doi:10.1016/0016-7037(79)90095-4

Gelesh, L., K. Marshall, W. Boicourt, and L. Lapham. 2016. Methane concentrations increase in bottom waters during summertime anoxia in the highly eutrophic estuary, Chesapeake Bay, U.S.A. Limnol. Oceanogr. **61**: S253–S266. doi:10.1002/lno.10272

Grant, N. J., and M. J. Whiticar. 2002. Stable carbon isotopic evidence for methane oxidation in plumes above Hydrate Ridge, Cascadia Oregon Margin. Global Biogeochem. Cycles **16**: 71-1-71–13. doi:10.1029/2001gb001851

Grégoire, M., V. Garçon, H. Garcia, and others. 2021. A Global Ocean Oxygen Database and Atlas for Assessing and Predicting Deoxygenation and Ocean Health in the Open and Coastal Ocean. Front. Mar. Sci. **8**. doi:10.3389/fmars.2021.724913

Hagens, M., C. P. Slomp, F. J. R. Meysman, D. Seitaj, J. Harlay, A. V. Borges, and J. J. Middelburg. 2015. Biogeochemical processes and buffering capacity concurrently affect acidification in a seasonally hypoxic coastal marine basin. Biogeosciences **12**: 1561–1583. doi:10.5194/bg-12-1561-2015

Haroon, M. F., S. Hu, Y. Shi, M. Imelfort, J. Keller, P. Hugenholtz, Z. Yuan, and G. W. Tyson.

2013. Anaerobic oxidation of methane coupled to nitrate reduction in a novel archaeal lineage. Nature **500**: 567–570. doi:10.1038/nature12375

Imboden, D. M., and A. Wüest. 1995. Mixing Mechanisms in Lakes. Phys. Chem. Lakes **@article{j**: 83–138. doi:10.1007/978-3-642-85132-2_4

IPCC. 2007. Climate Change 2007: : Synthesis Report. Contribution of Working Groups I, II and III to the Fourth Assessment Report of the Intergovernmental Panel on Climate Change. [Core Writing Team, Pachauri, R.K and Reisinger, A. (eds.)] . IPCC, Geneva, Switzerland. 104 pp.

Jähne, B., G. Heinz, and W. Dietrich. 1987. Measurement of the diffusion coefficients of sparingly soluble gases in water. J. Geophys. Res. Ocean. **92**: 10767–10776. doi:10.1029/JC092iC10p10767

Jørgensen, B. B., F. Beulig, M. Egger, C. Petro, C. Scholze, and H. Røy. 2019. Organoclastic sulfate reduction in the sulfate-methane transition of marine sediments. Geochim. Cosmochim. Acta **254**: 231–245. doi:10.1016/j.gca.2019.03.016

Joye, S. B., A. Boetius, B. N. Orcutt, J. P. Montoya, H. N. Schulz, M. J. Erickson, and S. K. Lugo. 2004. The anaerobic oxidation of methane and sulfate reduction in sediments from Gulf of Mexico cold seeps. Chem. Geol. **205**: 219–238. doi:10.1016/j.chemgeo.2003.12.019

Judd, A., G. Davies, J. Wilson, R. Holmes, G. Baron, and I. Bryden. 1997. Erratum : Contributions to atmospheric methane by natural seepages on the U.K continental shelf [Mar. Geol. 137 (1997) p165-189]. Mar. Geol. **Vol. 140**: 427–455. doi:10.1016/S0025-3227(96)00087-4

Knittel, K., and A. Boetius. 2009. Anaerobic oxidation of methane: progress with an unknown process. Annu. Rev. Microbiol. **63**: 311–334. doi:10.1146/annurev.micro.61.080706.093130

Kunpeng, Z., Z. Nan, X. Xuemei, Z. Lingxi, and W. Juying. 2019. Bubble-mediated methane release from polluted Dalian Bay in China in summer, 2016. Cont. Shelf Res. **185**: 51–56. doi:10.1016/j.csr.2018.11.009

Lan, X., K. W. Thoning, and E. J. Dlugokencky. 2023. Trends in globally-averaged CH4, N2O, and SF6 determined from NOAA Global Monitoring Laboratory measurements. Glob. Monit. Lab. **6**. doi:10.15138/P8XG-AA10

Leifer, I., and R. K. Patro. 2002. The bubble mechanism for methane transport from the shallow sea bed to the surface: A review and sensitivity study. Cont. Shelf Res. **22**: 2409–2428. doi:10.1016/S0278-4343(02)00065-1

Lenstra, W. K., N. A. G. M. Van Helmond, P. Dalcin Martins, A. J. Wallenius, M. S. M. Jetten, and C. P. Slomp. 2023. Gene-based modeling of methane oxidation in coastal sediments: constraints on the efficiency of the microbial methane filter.doi:10.1021/acs.est.3c02023

Lenstra, W. K., N. A. G. M. van Helmond, O. M. Żygadłowska, R. van Zummeren, R. Witbaard, and C. P. Slomp. 2022. Sediments as a Source of Iron, Manganese, Cobalt and Nickel to Continental Shelf Waters (Louisiana, Gulf of Mexico). Front. Mar. Sci. **9**: 1–32. doi:10.3389/fmars.2022.811953

Lenstra, W. K., M. Hermans, M. J. M. Séguret, R. Witbaard, S. Severmann, T. Behrends, and C. P. Slomp. 2021. Coastal hypoxia and eutrophication as key controls on benthic release and water column dynamics of iron and manganese. Limnol. Oceanogr. **66**: 807–826. doi:10.1002/lno.11644

Leonte, M., B. Wang, S. A. Socolofsky, S. Mau, J. A. Breier, and J. D. Kessler. 2018. Using Carbon Isotope Fractionation to Constrain the Extent of Methane Dissolution Into the Water Column Surrounding a Natural Hydrocarbon Gas Seep in the Northern Gulf of Mexico. Geochemistry, Geophys. Geosystems **19**: 4459–4475. doi:10.1029/2018GC007705

Leu, A. O., C. Cai, S. J. Mcilroy, S. Hu, G. W. Tyson, and G. W. Tyson. 2020. Anaerobic methane oxidation coupled to manganese reduction by members of the Methanoperedenaceae. ISME J. 1030–1041. doi:10.1038/s41396-020-0590-x

Li, B., Y. Tao, Z. Mao, and others. 2023. Iron oxides act as an alternative electron acceptor for aerobic methanotrophs in anoxic lake sediments. Water Res. **234**: 119833. doi:10.1016/j.watres.2023.119833

Martens, C. S., and J. Val Klump. 1980. Biogeochemical cycling in an organic-rich coastal marine basin-I. Methane sediment-water exchange processes. Geochim. Cosmochim. Acta **44**: 471–490. doi:10.1016/0016-7037(80)90045-9

Mau, S., J. Blees, E. Helmke, H. Niemann, and E. Damm. 2013. Vertical distribution of methane oxidation and methanotrophic response to elevated methane concentrations in stratified waters of the Arctic fjord Storfjorden (Svalbard, Norway). Biogeosciences **10**: 6267–6268. doi:10.5194/bg-10-6267-2013

McGinnis, D. F., J. Greinert, Y. Artemov, S. E. Beaubien, and A. Wüest. 2006. Fate of rising methane bubbles in stratified waters: How much methane reaches the atmosphere? J. Geophys. Res. Ocean. **111**. doi:10.1029/2005JC003183

Millero, F. J. 1991. The Oxidation of H 2 S with O 2 in the Black Sea. Black Sea Oceanogr. 205–227. doi:10.1016/S0198-0149(10)80028-7

Naqvi, S. W. A., H. W. Bange, L. FarÃ-As, P. M. S. Monteiro, M. I. Scranton, and J. Zhang. 2010. Marine hypoxia/anoxia as a source of CH 4 and N 2O. Biogeosciences **7**: 2159–2190. doi:10.5194/bg-7-2159-2010

Nijman, T. P. A., A. M. Amado, P. L. E. Bodelier, and A. J. Veraart. 2022. Relief of Phosphate Limitation Stimulates Methane Oxidation. Front. Environ. Sci. **10**: 1–8. doi:10.3389/fenvs.2022.804512

Ostrovsky, I., D. F. Mcginnis, L. Lapidus, and W. Eckert. 2008. Quantifying gas ebullition

with echosounder: The role of methane transport by bubbles in a medium-sized lake. Limnol. Oceanogr. Methods **6**: 105–118. doi:10.4319/lom.2008.6.105

Padilla, C. C., A. D. Bertagnolli, L. A. Bristow, N. Sarode, J. B. Glass, B. Thamdrup, and F. J. Stewart. 2017. Metagenomic binning recovers a transcriptionally active gammaproteobacterium linking methanotrophy to partial denitrification in an anoxic oxygen minimum zone. Front. Mar. Sci. **4**: 1–15. doi:10.3389/fmars.2017.00023

Padilla, C. C., L. A. Bristow, N. Sarode, and others. 2016. NC10 bacteria in marine oxygen minimum zones. ISME J. **10**: 2067–2071. doi:10.1038/ismej.2015.262

Pilson, M. E. Q. 2013. An introduction to the chemistry of the sea, Cambridge University Press.

Read, J. S., D. P. Hamilton, A. R. Desai, and others. 2012. Lake-size dependency of wind shear and convection as controls on gas exchange. Geophys. Res. Lett. **39**: 1–5. doi:10.1029/2012GL051886

Reeburgh, W. S. 2007. Oceanic methane biogeochemistry. Chem. Rev. **107**: 486–513. doi:10.1021/cr050362v

Reeburgh, W. S., B. B. Ward, S. C. Whalen, K. A. Sandbeck, K. A. Kilpatrickt, and L. J. Kerkhof. 1991. Black Sea methane geochemistry. Deep Sea Res. Part A. Oceanogr. Res. Pap. **38**: S1189--S1210. doi:10.1016/S0198-0149(10)80030-5

Reindl, A. R., and J. Bolałek. 2014. Methane flux from sediment into near-bottom water and its variability along the Hel Peninsula-Southern Baltic Sea. Cont. Shelf Res. **74**: 88–93. doi:10.1016/j.csr.2013.12.006

Reis, P. C. J., C. Ruiz-González, S. Crevecoeur, C. Soued, and Y. T. Prairie. 2020. Rapid shifts in methanotrophic bacterial communities mitigate methane emissions from a tropical hydropower reservoir and its downstream river. Sci. Total Environ. **748**: 141374. doi:10.1016/j.scitotenv.2020.141374

Rosentreter, J. A., A. V Borges, B. R. Deemer, and others. 2021. Half of global methane

emissions come from highly variable aquatic ecosystem sources. Nat. Geosci. **14**: 225–230. doi:10.1038/s41561-021-00715-2

Sapart, C. J., C. Van Der Veen, I. Vigano, and others. 2011. Simultaneous stable isotope analysis of methane and nitrous oxide on ice core samples. Atmos. Meas. Tech. **4**: 2607–2618. doi:10.5194/amt-4-2607-2011

Saunois, M., A. R. Stavert, B. Poulter, and others. 2020. The global methane budget 2000--2017. Earth Syst. Sci. data **12**: 1561–1623. doi:10.5194/essd-12-1561-2020

Schmale, O., J. Schneider Von Deimling, W. Gülzow, G. Nausch, J. J. Waniek, and G. Rehder. 2010. Distribution of methane in the water column of the Baltic Sea. Geophys. Res. Lett. **37**: 1–5. doi:10.1029/2010GL043115

Schmid, M., I. Ostrovsky, and D. F. McGinnis. 2017. Role of gas ebullition in the methane budget of a deep subtropical lake: What can we learn from process-based modeling? Limnol. Oceanogr. **62**: 2674–2698. doi:10.1002/lno.10598

Sivan, O., M. Adler, A. Pearson, F. Gelman, I. Bar-Or, S. G. John, and W. Eckert. 2011. Geochemical evidence for iron-mediated anaerobic oxidation of methane. Limnol. Oceanogr. **56**: 1536–1544. doi:10.4319/lo.2011.56.4.1536

Soetaert, K., T. Petzoldt, and R. W. Setzer. 2010. Solving differential equations in R: package deSolve. J. Stat. Softw. **33**: 1–25. doi:10.18637/jss.v033.i09

Solorzano, L. 1969. Determination of ammonia in natural waters by the phenolhypochlorite method. This research was fully supported by US Atomic Energy Commission Contract No. ATS (11-1) GEN 10, PA 20. Limnol. Oceanogr. **14**: 799–801. doi:10.4319/lo.1969.14.5.0799

Steinle, L., J. Maltby, T. Treude, and others. 2017. Effects of low oxygen concentrations on aerobic methane oxidation in seasonally hypoxic coastal waters. Biogeosciences **14**: 1631–1645. doi:10.5194/bg-14-1631-2017

Steinsdóttir, H. G. R., C. Schauberger, S. Mhatre, B. Thamdrup, and L. A. Bristow. 2022. Aerobic and anaerobic methane oxidation in a seasonally anoxic basin. Limnol. Oceanogr. **67**: 1257–1273. doi:10.1002/lno.12074

Thamdrup, B., H. G. R. Steinsdóttir, A. D. Bertagnolli, C. C. Padilla, N. V. Patin, E. Garcia-Robledo, L. A. Bristow, and F. J. Stewart. 2019. Anaerobic methane oxidation is an important sink for methane in the ocean's largest oxygen minimum zone. Limnol. Oceanogr. **64**: 2569–2585. doi:10.1002/lno.11235

Venetz, J., O. M. Żygadłowska, W. K. Lenstra, N. A. G. M. van Helmond, G. H. L. Nuijten, A. J. Wallenius, P. Dalcin Martins, C. P. Slomp, M. S. M. Jetten, A. J. Veraart. 2023a. Versatile methanotrophs form an active methane biofilter in the oxycline of a seasonally stratified coastal basin. Environ. Microbiol. 1–12. doi:10.1111/1462-2920.16448

Venetz, J., O. M. Żygadłowska, N. Dotsios, W. K. Lenstra, R. Klomp, A. Wallenius, N. A. G. M. van Helmond, C. P. Slomp, M. S. M. Jetten, A. J. Veraart. 2023b. Seasonal dynamics of the microbial methane filter in the water column of a eutrophic coastal basin.

Wallace, P. J., G. R. Dickens, C. K. Paull, and W. Ussler. 2000. Effects of core retrieval and degassing on the carbon isotope composition of methane in gas hydrate-and free gas-bearing sediments from the Blake Ridge. Proc. Ocean Drill. program. Sci. Results **164**: 101–112. doi:10.2973/odp.proc.sr.164.209.2000

Wallenius, A. J., P. Dalcin Martins, C. P. Slomp, and M. S. M. Jetten. 2021. Anthropogenic and Environmental Constraints on the Microbial Methane Cycle in Coastal Sediments. Front. Microbiol. **12**. doi:10.3389/fmicb.2021.631621

Wanninkhof, R. 2014. Relationship between wind speed and gas exchange over the ocean revisited. Limnol. Oceanogr. Methods **12**: 351–362. doi:10.4319/lom.2014.12.351

Weber, T., N. A. Wiseman, and A. Kock. 2019. Global ocean methane emissions dominated by shallow coastal waters. Nat. Commun. **10**: 1–10. doi:10.1038/s41467-019-12541-7

Wiesenburg, D. A., and N. L. Guinasso. 1979. Equilibrium Solubilities of Methane, Carbon Monoxide, and Hydrogen in Water and Sea Water. J. Chem. Eng. Data **24**: 356–360. doi:10.1021/je60083a006

Wik, M., P. M. Crill, R. K. Varner, and D. Bastviken. 2013. Multiyear measurements of ebullitive methane flux from three subarctic lakes. J. Geophys. Res. Biogeosciences **118**: 1307–1321. doi:10.1002/jgrg.20103

Żygadłowska, O. M., J. Venetz, R. Klomp, and others. 2023. Pathways of methane removal in the sediment and water column of a seasonally anoxic eutrophic marine basin. Front. Mar. Sci. **10**: 1–15. doi:10.3389/fmars.2023.1085728

Data Availability Statement

The original contributions presented in the study are included in the article/Supplementary Material and in the Zenodo repository (10.5281/zenodo.10034519), further inquiries can be directed to the corresponding author.

High methane emissions from a eutrophic marine coastal basin driven by bubble release from the sediment

Olga M. Żygadłowska[1], Jessica Venetz[2], Wytze K. Lenstra[1,2], Niels A.G.M. van Helmond[1,2], Robin Klomp[1,2], Thomas Röckmann[3], Annelies J. Veraart[4], Mike S.M. Jetten[2], Caroline P. Slomp[1,2]

[1] Department of Earth Sciences - Geochemistry, Utrecht University, The Netherlands

[2] Department of Microbiology, Radboud Institute for Biological and Environmental Sciences, Radboud University, Nijmegen, The Netherlands

[3] Institute for Marine and Atmospheric Research Utrecht, Utrecht University, Utrecht, The Netherlands

[4] Department of Aquatic Ecology and Environmental Biology, Radboud Institute for Biological and Environmental Sciences, Radboud University, Nijmegen, The Netherlands

Correspondence:

Olga M. Żygadłowska

o.m.zygadlowska@uu.nl

Supplementary information

The data presented in this study are available in the Zenodo repository, doi: 10.5281/zenodo.10034519.

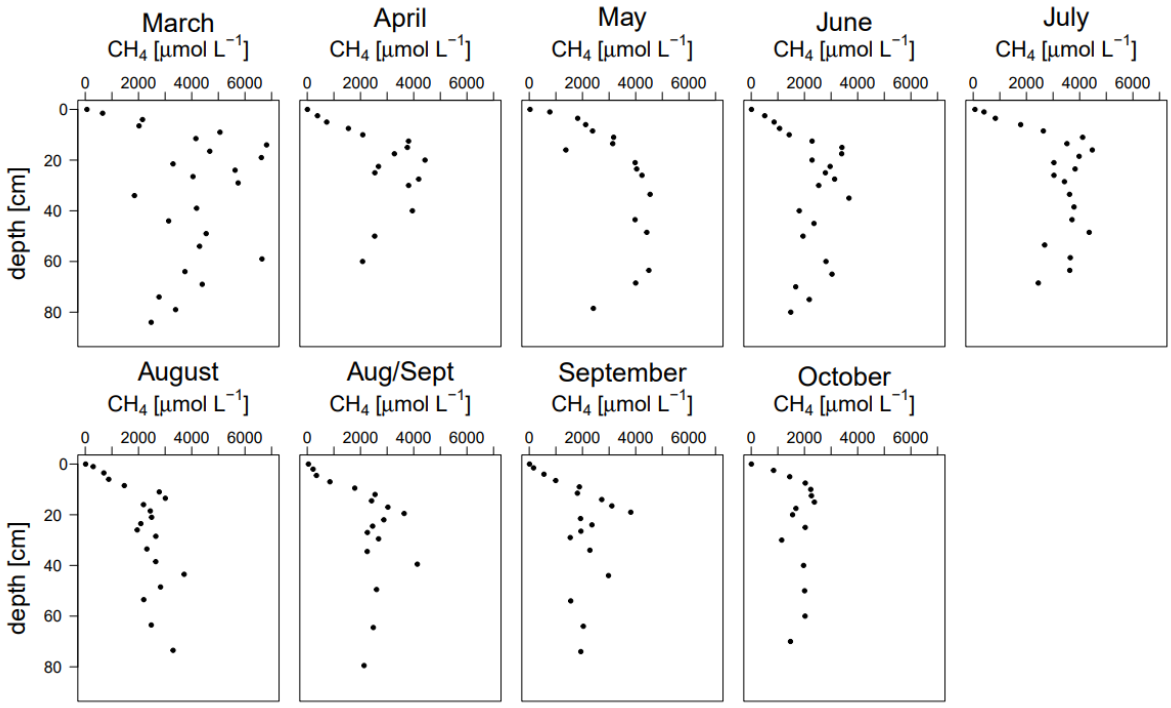

Figure S1. Porewater methane concentrations at Scharendijke for all the sampled months in 2021.

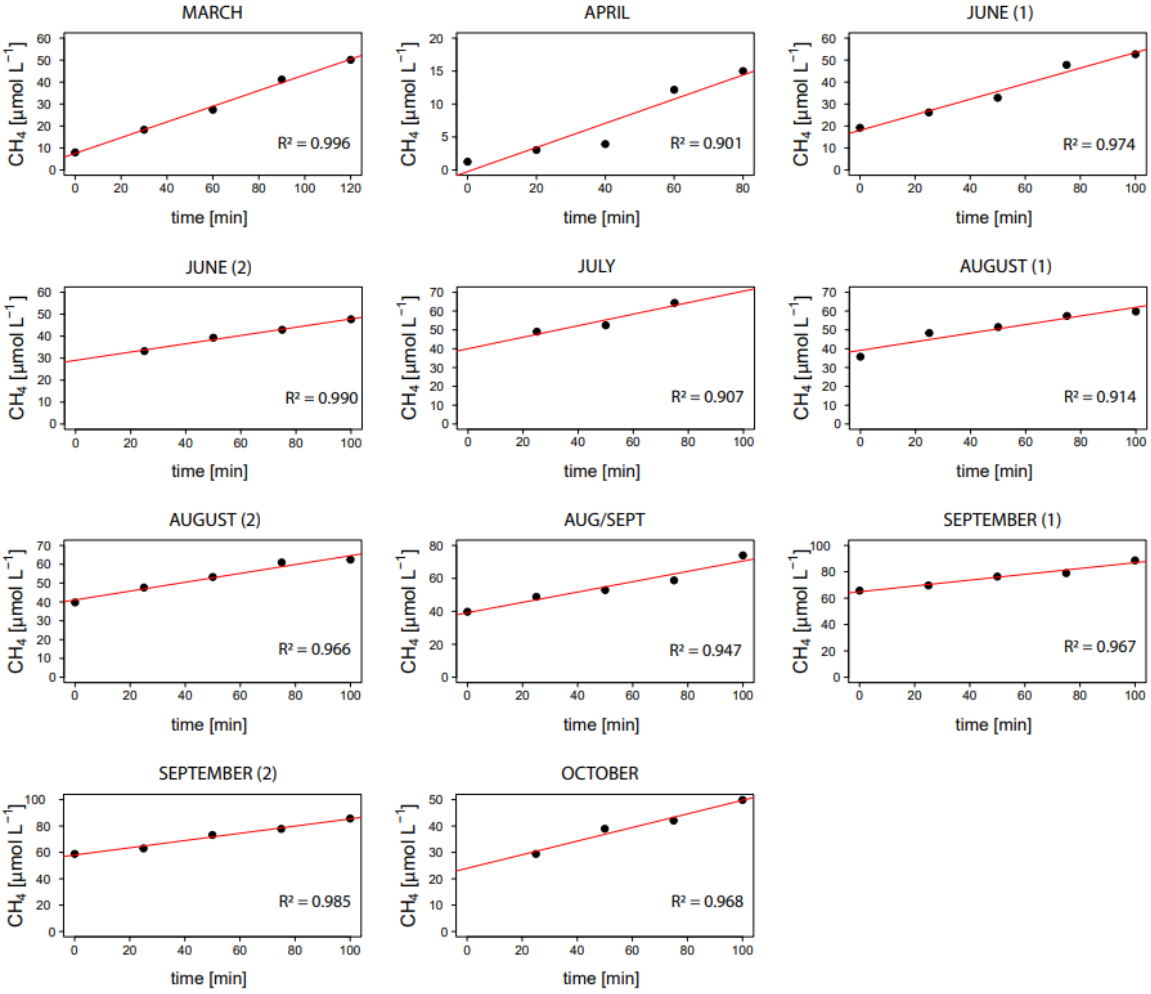

Figure S2. Methane concentrations in the benthic lander chamber versus time. Fluxes were calculated using linear regression. The values of R^2 were always above 0.9.

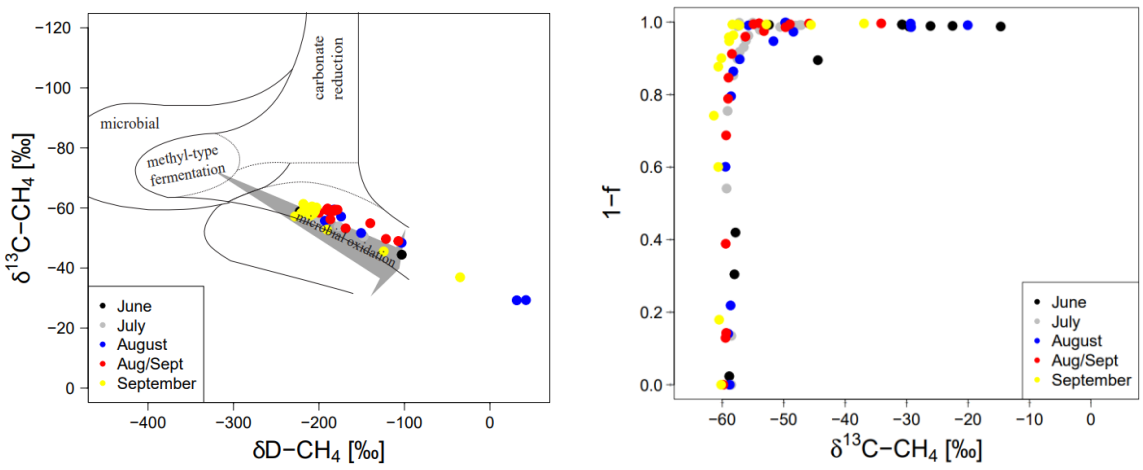

Figure S3. A) Isotopic composition of methane (δ^{13}C-CH_4 and δD-CH_4) modified after (Whiticar, 1999; Egger et al., 2017). The grey arrow indicates the direction of the shift in isotopic composition due to microbial methane oxidation (Whiticar, 1999). B) The fraction of methane removed (1-f) as a function of δ^{13}C of methane where f stands for the concentration of methane in a sample relative to the bottom water methane, illustrating the strong effect of the bubble dissolution on the isotopic signature.

Table S1. Fractionation factors

Date	**Fractionation factor**
June	1.011
July	1.006
August	1.014
Aug/Sept	1.009
September	1.009

Table S2. Bubble fluxes estimated based on events when bubbles entered the floating chamber during measurements. The bubbles were caught in the chamber on 5 separate occasions throughout the year.

Sampling date	Bubble flux [mmol m^{-2} d^{-1}]
April	63.6
June	8.7
Aug/Sept	18.7
September	245.3
October	0.5
Average	67.3

The contribution of methane bubble dissolution to dissolved methane concentrations in the surface waters

To calculate the contribution of bubble dissolution to total methane concentrations at 5 m we applied a simple mass balance:

$$\boldsymbol{C_s Iso_s = C_{diff} Iso_{diff} + C_{bubb} Iso_{bubb}}$$

Where C_s, Iso_s, C_{diff}, Iso_{diff}, C_{bubb}, Iso_{bubb} are the concentrations and isotopic signatures of methane, respectively, in the surface waters, supplied from diffusion and supplied from bubble dissolution. To calculate the ratio in the mass balance we assumed the depth with the strongest isotopic enrichment represents methane supplied from diffusion and the depth closest to the sediment-water interface represents methane supplied from bubble dissolution.

Water column methane transport by turbulent diffusion

To model the water column methane concentrations with the assumption that the only parameter controlling methane distribution is turbulent diffusion the following equation was applied (Crank, 1975):

$$C(z,t) = C_O \, erfc \, \frac{z}{2\sqrt{(K_z t)}}$$

where C is the methane concentration in the water column in μmol L^{-1} as a function of time (t) and depth (z), C_O is the methane concentration close to the sediment-water interface in μmol L^{-1} and K_Z is the turbulent diffusion coefficient in m^{-2} d^{-1}. Time was determined as the number of days between the samplings.

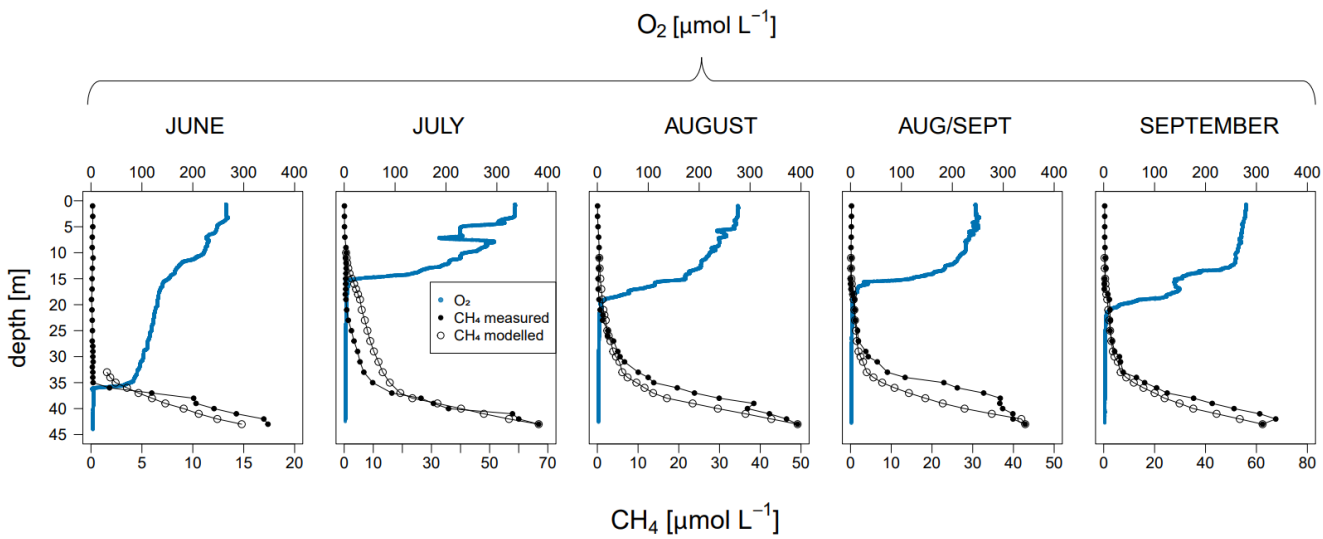

Figure S4. Methane concentrations modelled assuming transport by turbulent diffusion only. Oxygen and methane profiles in the water column from Figure 3 for reference.